

# The optically–dark side of galaxy formation

Bruno Guiderdoni<sup>1</sup>, François R. Bouchet<sup>1</sup>, Jean–Loup Puget<sup>2</sup>,

Guilaine Lagache<sup>2</sup> & Eric Hivon<sup>3</sup>

<sup>1</sup> *Institut d’Astrophysique de Paris, CNRS, 98bis Boulevard Arago, F–75014 Paris*

<sup>2</sup> *Institut d’Astrophysique Spatiale, Bât. 121, Université Paris XI, F–91405 Orsay Cedex*

<sup>3</sup> *Theoretical Astrophysics Center, Juliane Maries Vej 30, DK–2100 Copenhagen*

In this letter, we estimate how much starlight was absorbed by dust and released in the infrared during the formation of galaxies. New constraints are set on this so–far hidden history by the recent detection of the Cosmic Infrared Background (CIB) built up from the accumulated light of faint sources (and revisited here). By means of a semi-analytical model of hierarchical galaxy formation, we estimate the population of dust–enshrouded starburst galaxies fitting the CIB. It is argued that a deep ISO survey at  $\lambda_{eff} = 175\mu\text{m}$  could already detect these sources and help close the gap in our understanding of the history of light in the Universe.

UV/optical observers of high–redshift objects have recently achieved a spectacular breakthrough [1, 2]. Their results match a scenario where star formation in bursts triggered by interaction/merging consumes the gas content of galaxies as time goes on. Semi–analytical

models of hierarchical galaxy formation substantiate this view and may lead one to conclude that the bulk of star formation has been seen [3]. Nevertheless, the corrections for dust extinction are rather uncertain and an upward revision of the high-redshift SFR deduced from UV/optical observations by factors of a few is quite possible. While only one third of the luminosity emitted by galaxies at redshifts  $z \simeq 0$  is radiated in the IR [4], we have so far no measurement at higher  $z$ . The deepest counts at  $60 \mu\text{m}$  with the Infrared Astronomical Satellite (IRAS) probe flux levels  $> 60 \text{ mJy}$  [5], corresponding to an average  $z$  of only 0.1 [6]. Most predictions at fainter levels are based on mere extrapolations of the luminosity and/or number density evolution derived from these shallow counts. More positively, the analysis of the COBE/FIRAS data in the  $100 \mu\text{m} - 2 \text{ mm}$  wavelength range by Puget and coworkers has revealed an isotropic residual which could be the long-sought CIB due to the line-of-sight accumulation of emissions by faint extragalactic sources [7]. We hereafter briefly review the observational issue before we draw the consequences of this new constraint on the history of galaxy formation.

At the wavelengths probed by FIRAS, the interplanetary component is small and easily removed [8]. The critical component comes from interstellar dust mixed with the different gas phases of the interstellar medium. The correlation of FIRAS spectra with the 21 cm HI interstellar emission [9] along lines-of-sight with HI column densities  $N_{\text{HI}} \leq 4.5 \times 10^{20} \text{ cm}^{-2}$  is described with little residual by a single spectrum with  $T = 17.5 \text{ K}$  and  $\nu^2$  emissivity [10]. Part of the long-wavelength excess over this simple model increases with HI column density and can be linked to dust emission associated with ionized and molecular hydrogen. The inset in fig.1 shows that the remaining isotropic component dominates the emission in regions with very low HI column densities ( $N_{\text{HI}} \leq 1 \times 10^{20} \text{ cm}^{-2}$ ). Its spectrum is very similar to the isotropic component found by Puget *et al.* [7] in a much larger fraction of the sky. This demonstrates that it cannot be due to artifacts in the removal of interstellar emission. Systematic errors due to subtraction are negligible, and the detection of the average  $600 - 900 \mu\text{m}$  emission is significant at the  $\sim 6\sigma$  level. Fig.1 also shows that the CIB energy

per frequency decade at  $200\ \mu\text{m}$  is comparable to that of the “Cosmic Optical Background” (COB) estimated by summing up faint galaxy counts down to the Hubble Deep Field (HDF) limit.

Semi-analytical models have been rather successful in reproducing the overall properties of galaxies in the optical range, in spite of some difficulties [11, 12, 3]. In order to constrain the sources contributing to the CIB, we elaborated an extension of this type of method to the IR/submm range. Details of the modelling, and extensive predictions are given elsewhere [13, 14], but the general idea is the following. Small fluctuations in the high- $z$  Universe grow by gravitational instability until they form dense clumps where the baryonic gas is collisionally heated. Where the density and temperature are appropriate, gas cools by emitting radiation, and the baryons pile up in cold cores whose final radii are set by angular-momentum conservation. Simultaneously, larger clumps form and encompass/accrete the previous generation of small clumps. Stars form in the cores and enrich the primordial gas via supernova ejecta. Part of the starlight is absorbed by various dust components which re-radiate at longer wavelengths according to characteristic IR spectra.

Specifically, we assume a standard Cold Dark Matter cosmological scenario ( $H_0 = 50\ \text{km s}^{-1}\ \text{Mpc}^{-1}$ ,  $\Omega_0 = 1$ ,  $\Lambda = 0$ ,  $\Omega_b = 0.05$ ,  $\sigma_8 = 0.67$ ). Stars form in cold cores according to Salpeter’s initial mass function (with slope  $s = 1.35$ ) and star formation rates (SFR) proportional to the cold gas contents, with characteristic time scales derived from the core dynamical times as  $t_\star = \beta t_{dyn}$ . In our reference model (hereafter model A), we consider a mix of two broad types of populations, one with a quiet star formation rate, the other proceeding in bursts. In the quiet mode, we choose  $\beta = 100$  which reproduces the observational distribution of gas consumption time scales in disk galaxies [15]. For the burst mode, we take  $\beta = 10$ , and an involved mass fraction  $f_{burst} = A(1+z)^5$ , as suggested by the increasing fraction of pairs and blue objects showing interaction/merger features at larger  $z$  [16, 17, 18]. We set  $A = 0.04$  in order to fit the SFR density at low  $z$ , resulting in an “all-burst” behavior at  $z \geq 0.8$ . This population of “mild starbursts” and “luminous UV/IR galaxies” (LIGs)

dominate the COB (fig.1). The range of IR-to-blue luminosity ratios is characteristic of blue-band selected samples [19] like the Canada-France Redshift Survey (selected in the observer-frame  $I_{AB}$  band, roughly corresponding to the  $B$  band at  $z \sim 1$ ), or the high- $z$  HDF galaxies. Fig.1 displays the predicted CIB, which is clearly barely compatible with the observed CIB whose mean amplitude is twice higher. Fig.2a shows the corresponding cosmic SFR history which fits the strong evolution at  $z \leq 1$ , and predicts a high- $z$  evolution closer to the one derived from photometric estimates of redshifts rather than that from Lyman-continuum drop-outs. As a consequence of the high SFR, the gas content strongly evolves between  $z \sim 2$  and 0, as shown in fig.2b.

In order to assess how much star formation might be hidden by dust shrouds, we consider an *additional* population, similar to “ultra-luminous IR galaxies” (ULIGs) [26]. We maximize their IR luminosity by assuming that all the energy available from stellar nucleosynthesis ( $0.007xMc^2$ ) is radiated by massive stars ( $\langle x \rangle = 0.40$ ) in a heavily-extinguished medium. We distribute this population of ULIGs in two ways. Model B has a 5 % constant mass fraction of ULIGs at all  $z$ , mimicking a scenario of continuous bulge formation as the end-product of interaction and merging. The IRAS 60  $\mu\text{m}$  counts of fig.3a limit the *local* mass fraction to  $\leq 7$  %, while the fit of the CIB in fig.1 would rather suggest a fraction amounting to 10 % at larger distances. In model C, 90 % of all galaxies forming at  $z_{for} \geq 3.5$  are ULIGs, mimicking a strong episode of bulge formation. Of course, these two models are only illustrative, and a combination of these solutions would also fit the CIB. For instance, a model with an ULIG fraction increasing from 5 % at  $z = 0$  to 50 % at high  $z$  would both fit the 60  $\mu\text{m}$  counts and the average value of the 200 – 900  $\mu\text{m}$  CIB. It is clear from fig.2c that none of the optical data reflects the large differences between these scenarios, although the fraction of light in the IR varies widely at high  $z$ .

Fig.3a compares the predicted counts of our models. The 60  $\mu\text{m}$  band is not discriminating. In the submm range, the upward deviation is due to the contribution of the redshifted 100  $\mu\text{m}$  maximum of the IR energy distribution. This redshifting of steep spectra counter-

balances the distance dimming and can make high- $z$  objects *easier* to detect. Submm observations are thus quite sensitive to the high- $z$  history. Fig.3b shows that, at 200  $\mu\text{m}$ , 10–100 mJy sources (contributing to 15 % of the background) are mostly located at  $z \sim 0.5 - 2.5$ , while at 60  $\mu\text{m}$ , and at the typical sensity level of IRAS surveys, the sources are indeed located mostly at very low  $z$ .

The C160 filter of the ISOPHOT instrument on-board the Infrared Space Observatory (ISO) has an effective wavelength  $\lambda_{eff} \simeq 175 \mu\text{m}$  for typical spectra of distant galaxies, and 10 mJy *rms* noise fluctuation per 1.5' pixel is reachable after integration times larger than  $\sim 256$  s per pixel. Could small-scale cirrus fluctuations hide the sources and the fluctuations of the background they induce ? Fig.3c compares the expected power spectra of 1) cirrus fluctuations in regions of various HI column densities; 2) the background once sources above the confusion limit have been removed; 3) the detector noise. In clean regions of the sky ( $N_{HI} \leq 1 \times 10^{20} \text{cm}^{-2}$ ), a survey with 10 mJy *rms* sensitivity should not only detect most sources above the confusion limit but could also see white noise fluctuations due to the unresolved background in excess of the detector contribution. Since model C has  $6.3 \times 10^5$  sources/sr with fluxes  $> 30$  mJy, a deep survey of a  $\sim 1000 \text{ arcmin}^2$  field might begin to “break” the CIB into  $\sim 50$  discrete sources. If detected, the level of the background can constrain the redshift distribution of the sources. Consequently, our knowledge of the optical/IR energy budget at  $z \sim 0.5 - 2.5$  should improve rapidly. We are about to start unveiling the optically-dark side of galaxy formation.

**Acknowledgments.** We are pleased to thank Dave Clements, François-Xavier Désert, and Bruno Maffei for their comments and suggestions.

## References

- [1] Lilly, S.J., Tresse, L., Hammer, F., Crampton, D., & Le Fèvre, O., 1995, ApJ **455**, 108
- [2] Williams, R.E., *et al.*, 1996, A.J. **112**, 1335

- [3] Baugh, C.M., Cole, S., Frenk, C.S., & Lacey, C.G. 1997, *preprint*
- [4] Soifer, B.T., & Neugebauer, G. 1991. *AJ*, **101**, 354
- [5] Hacking, P., & Houck, J.R., 1987, *ApJSS* **63**, 311
- [6] Ashby, M.L.N., Hacking, P.B., Houck, J.R., Soifer, B.T., & Weisstein, E.W., 1996, *ApJ* **456**, 428
- [7] Puget, J.L., Abergel, A., Boulanger, F., Bernard, J.P., Burton, W.B., *et al.*, 1996, *A & A* **308**, L5
- [8] Reach, W.T., *et al.* 1995, astro-ph 9504056
- [9] Hartmann, D., & Burton, W.B., 1995, *An Atlas of Galactic Neutral Hydrogen Emission*, Cambridge University Press
- [10] Boulanger, F., Abergel, A., Bernard, J.P., Burton, W.B., Désert, F.X., *et al.*, 1996, *A & A* **312**, 256
- [11] Lacey, C., & Silk, J. 1991. *ApJ*, **381**, 14
- [12] Kauffmann, G.A.M., White, S.D.M., & Guiderdoni, B. 1993. *MNRAS*, **264**, 201
- [13] Guiderdoni, B., Hivon, E., Bouchet, F.R., Maffei, B., 1997, *in preparation*
- [14] Hivon, E., Guiderdoni, B., Bouchet, F. 1997, *in preparation*
- [15] Kennicutt, R.C., Tamblyn, P., & Congdon, C.W. 1994. *ApJ*, **435**, 22
- [16] Zepf, S.E., & Koo, D.C. 1989. *ApJ*, **337**, 34
- [17] Burkey, J.M., Keel, W.C., Windhorst, R.A., Franklin, B.E. 1994, *ApJ* **429**, L13
- [18] Carlberg, R.G., Pritchet, C.J., Infante, L., 1994, *ApJ* **435**, 540
- [19] Soifer, B.T., Sanders, D.B., Madore, B.F., Neugebauer, G., Danielson, G.E., *et al.*, 1987, *ApJ* **320**, 238
- [20] Lilly, S.J., Le Fèvre, O., Hammer, F., & Crampton, D., 1996, *ApJ* **460**, L1
- [21] Sawicki, M.J., Lin, H., Yee, H.K.C., 1997, *AJ*, 113, 1
- [22] Madau, P., Ferguson, H.C., Dickinson, M.E., Giavalisco, M., Steidel, C.C., Fruchter, A., 1996, *MNRAS* **283**, 1388
- [23] Storrie-Lombardi, L.J., McMahon, R.G., Irwin, M.J., 1996, *MNRAS* **283**, L79
- [24] Briggs, F.H., & Rao, S. 1993. *ApJ* **417**, 494
- [25] Saunders, W., Rowan-Robinson, M., Lawrence, A., Efstathiou, G., Kaiser, N., Ellis, R.S., & Frenk, C.S. 1990. *MNRAS*, **242**, 318

- [26] Sanders, D.B., & Mirabel, I.F. 1996, ARAA, **34**, 749
- [27] Lonsdale, C.J., Hacking, P.B., Conrow, T.P., & Rowan–Robinson, M., 1990. ApJ, **358**, 60
- [28] Rowan–Robinson, M., Saunders, W., Lawrence, A., Leech, K., 1991, MNRAS **253**, 485
- [29] Bertin, E., Dennefeld, M., Moshir, M. 1997, A&A, *in press*
- [30] Gautier, T. N., III, Boulanger, F., Perault, M., & Puget, J. L., 1992, AJ, **103**, 1313

## Figure Captions

**Figure 1:** *Inset panel:* High-latitude COBE/FIRAS spectrum in regions with very low HI column densities (solid line) and residual spectrum after subtraction of HI and HII correlated emissions (dots). This component is likely to be the Cosmic Infrared Background (CIB). *Main panel:* The  $\pm 1\sigma$  error bars per point have been used to define an acceptable range for CIB predictions (thick solid lines). Solid triangles show the level of COBE/DIRBE residuals. The similar shapes of the residuals and dark sky suggest that the subtraction of foregrounds has been uncomplete and that the plotted values are upper limits. The solid hexagons show the Cosmic Optical Background (COB) obtained by summing up faint galaxy counts down to the Hubble Deep Field limit. Strictly speaking, this is only a lower limit of the actual COB, but the shallowing of the  $U$  and  $B$ -band counts suggests near-convergence at least at those wavelengths [2]. The solid, dotted and dashed lines show the predictions for our A, B, and C models respectively (see text). Fitting the mean CIB would require a 10 % ULIG mass fraction in the B model (and 30% at  $+1\sigma$  level), while the current IR counts limit the *local* fraction to  $\sim 7$  %.

**Figure 2:** Comparisons of the model evolution (with the same line coding as in fig.1) with available global data. *Panel a (top):* cosmic star-formation-rate comoving density as computed from rest-frame UV luminosity densities corrected for average extinction typical of LIGs, using a Salpeter's IMF of slope 1.35. The solid squares are derived from the rest-frame 2800 Å luminosity density in the Canada-France Redshift Survey, and local values are from the  $B$ -band luminosity function and average UV- $B$  colour [20]. The solid triangles come from a photometric-redshift analysis of the Hubble Deep Field [21], while the small open triangles are lower and upper values from the Hubble Deep Field with redshifts derived from Lyman-continuum drop-outs [22]. *Panel b (middle):* cold gas density parameter in Damped Lyman- $\alpha$  absorbers. Solid triangles: data without the APM QSO survey. Solid squares: data including the APM QSO survey. Open squares: tentative correction for selection effects



due to QSO obscuration [23]. Open triangle: local estimate from HI surveys [24]. *Panel c (bottom)*: rest-frame comoving luminosity density in UV (emissivities at 1600 Å and 2800 Å are similar). B, I and IR are for 4400 Å, 10000 Å and 60 μm. Solid squares: local and Canada–France Redshift Survey [20]. Solid triangle: 60 μm local density corresponding to one third of the light radiated in the IR [25]. Solid Hexagons: Hubble Deep Field with photometric redshifts [21]. Open squares: Hubble Deep Field with Lyman–continuum drop-outs [22]. The different UV and IR emissions mainly result from different IMF and extinction.

**Figure 3:** *Panel a (top)*: Predictions for differential counts normalized to Euclidean counts at 60, 200 and 550 μm. Data is shown for IRAS counts at 60 μm: open stars are for the Faint Source Survey [27], open squares are for the QMW survey [28], while the solid squares correspond to the North Ecliptic Pole Region [5]. The models (with similar line coding to previous figures) predict a 60 μm background fluctuation per beam in the Very Faint Source Survey (after removal of  $\geq 4\sigma_{tot} = 120$  mJy sources) at the level of 14.1 mJy (A), 16.0 mJy (B), and 14.3 mJy (C), while the measured 68 % quantile is  $30.1 \pm 1.2$  mJy [29]. With a 25 mJy *rms* instrumental noise and 6.5 mJy *rms* cirrus fluctuations [30], there is still room for a  $15.4^{+2.2}_{-2.5}$  mJy fluctuation due to sources, in good agreement with our estimates. Moreover, if the cirrus fluctuations are non-gaussian, the *rms* value strongly overestimates the 68 % quantile and can allow  $16.8^{+2.0}_{-2.3}$  mJy for source fluctuation. *Panel b (bottom left)*: redshift distributions for the flux ranges  $100 \text{ mJy} < S < 1 \text{ Jy}$  at 60 μm (typical of IRAS surveys) and  $10 \text{ mJy} < S < 100 \text{ mJy}$  at 200 μm (typical of ISOPHOT deep surveys). While the redshift distribution at 60 μm peaks at low  $z$ , 90 % of the sources in the 10 – 100 mJy flux range (contributing up to 15 % of the 200 μm CIB) are at  $z \sim 0.5 - 2.5$ . *Panel c (bottom right)*: comparison of predicted power spectra for observations in the ISO C160 filter. The cirrus fluctuations (thin lines) are described by a  $k^{-3}$  power law [30] with levels (from left to right) set by HI column densities respectively typical of the Lockman hole (minimum, 0.24 % of the sky), and of 4.6 %, & 21.8 % of the sky. The detector noise spectrum, assumed

to be white, has been projected on the sky for direct comparison with the other curves (i.e. after measurement, all displayed spectra are to be convolved with the observational beam – taken here to be a 1' FWHM gaussian – which brings back the observed noise spectrum to a flat, white noise curve). The exponential rise of the on-sky noise thus displays the effective range of available scales. Finally, the straight horizontal lines correspond to the theoretical backgrounds at the confusion limit (same coding as in fig.1), i.e. whose *rms* value equals one third of the limiting flux of all resolved and removed sources.

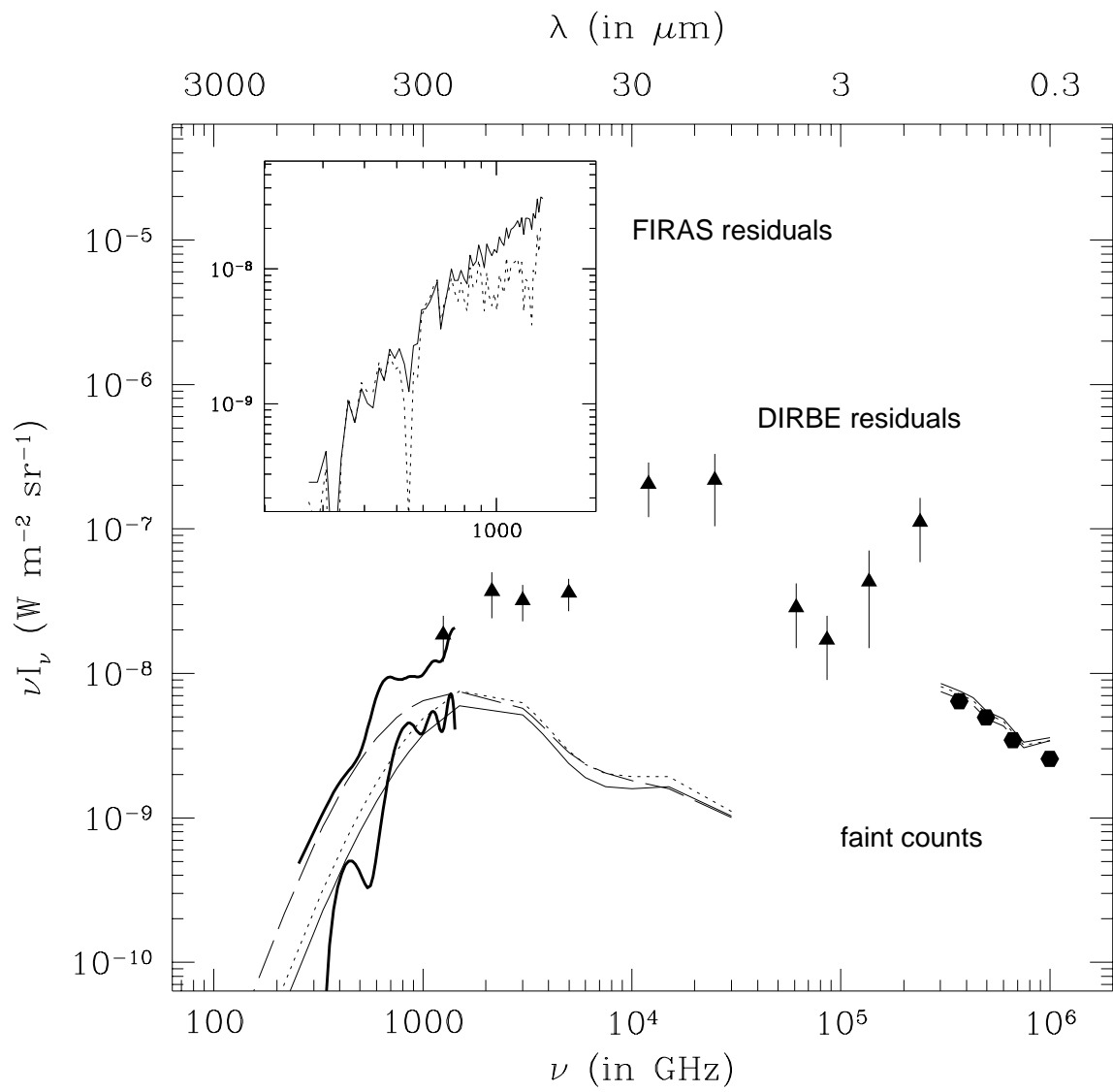


Figure 1:

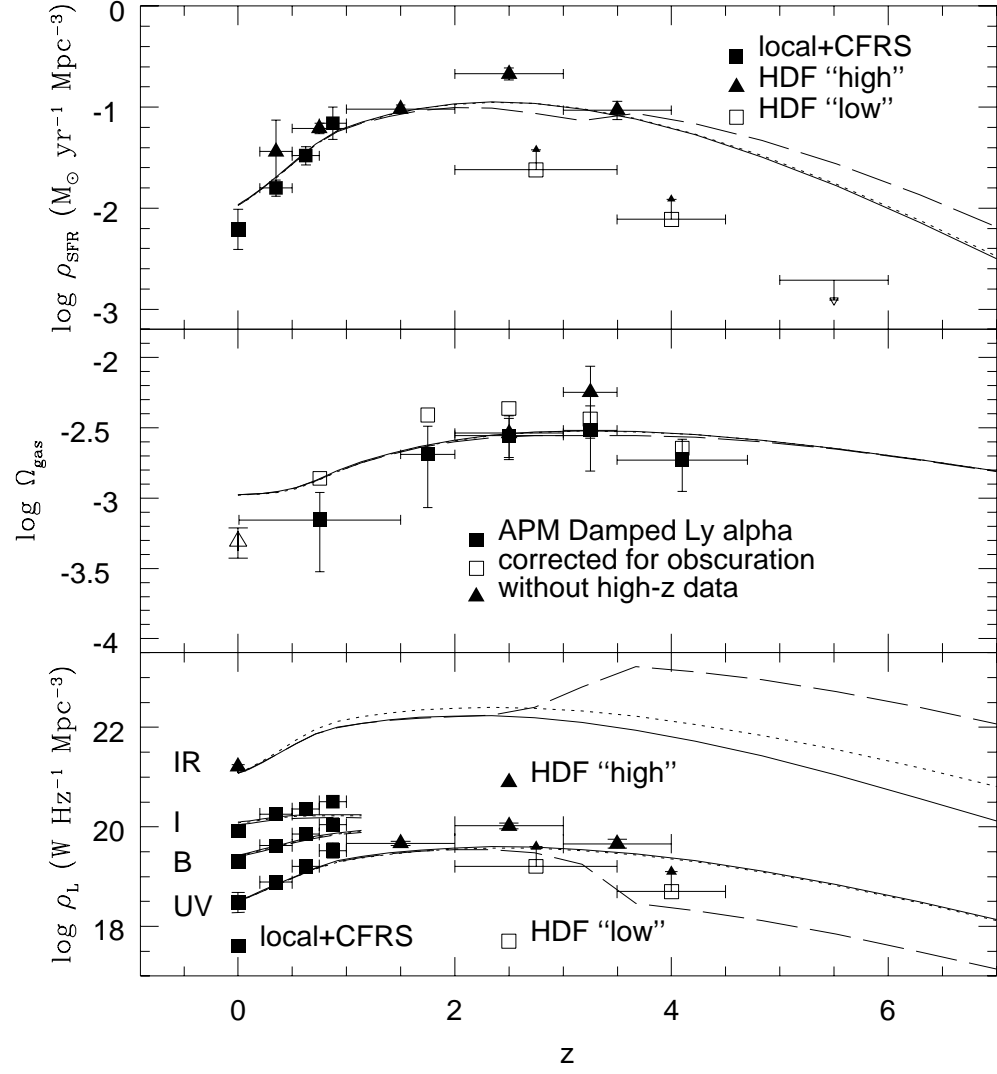


Figure 2:

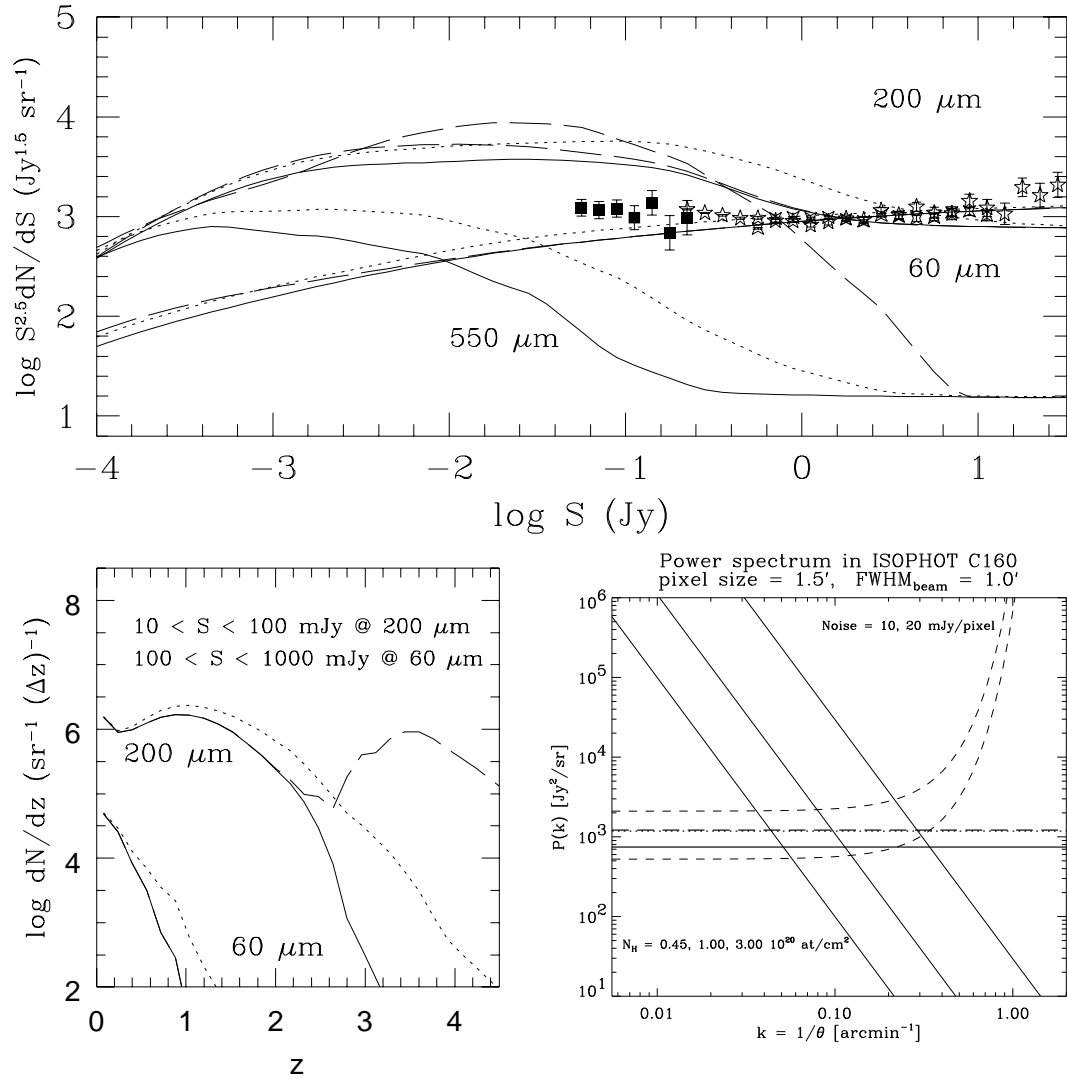


Figure 3: